Inorganic Chemistry

Article

pubs.acs.org/IC

$M_3(P_2O_7)_2^{2-}$-Type Open Frameworks Featuring $[M_2O_8]$ and $[M_3O_{12}]$ Multinuclear Transition-Metal Oxide Units. Serendipitous Synthesis of Six Polymorphic Salt-Inclusion Magnetic Solids: $Na_2M_3(P_2O_7)_2$·ACl (M = Mn, Fe; A = Rb, Cs) and $K_2M_3(P_2O_7)_2$·CsCl (M = Fe, Mn)

Jianhua Gao,[†,‡] Jian Li,[†] Dino Sulejmanovic,[§] and Shiou-Jyh Hwu*[,§,‡]

[†]School of Physics, Department of Materials Physics, Northwest University, Xi'an 710069, China

[§]Department of Chemistry, Clemson University, Clemson, South Carolina 29634-0973, United States

Supporting Information

ABSTRACT: Single crystals of six polymorphic salt-inclusion phosphates of the $A_2M_3(P_2O_7)_2$·A′Cl type, $Na_2Mn_3(P_2O_7)_2$·CsCl (**1**), $Na_2Mn_3(P_2O_7)_2$·RbCl (**2**), $Na_2Fe_3(P_2O_7)_2$·CsCl (**3**), $Na_2Fe_3(P_2O_7)_2$·RbCl (**4**), $K_2Mn_3(P_2O_7)_2$·CsCl (**5**), and $K_2Fe_3(P_2O_7)_2$·CsCl (**6**), were grown in reactive molten chloride flux media. Compounds **1**−**4** are isostructural and crystallize in the space group $C2/c$ (No. 15), while **5** and **6** crystallize in $P2/c$ (No. 13) and $P\bar{1}$ (No. 2), respectively. The title compounds have demonstrated an unprecedented versatility, where the $M_3(P_2O_7)_2^{2-}$ covalent open frameworks contain $[M_3O_{12}]$ (M = Mn^{2+}, Fe^{2+}) trimeric units in **1**−**4** and $[M_2O_8]$ dimers in **5** and **6**. These multinuclear, transition-metal oxide units are linked by Cl^- ions through the M−Cl bonds to form one-dimensional (1D) chains. The 1D chains and $[P_2O_7]$ groups share common O atoms to form the extended network. The $M_3(P_2O_7)_2^{2-}$ open-framework structures exhibit channels where the respective Na^+/K^+ ions and A′Cl salt (A′ = Rb, Cs) reside. Magnetic susceptibility of **2** and **4** suggests bulk antiferromagnetic properties as expected. The local structure and thermal decomposition are examined by IR and differential scanning calorimetry of representative compounds. The factors that determine the reticular chemistry of the $M_3(P_2O_7)_2^{2-}$ type are illustrated in terms of the inclusion of ionic lattices of different sizes and contents.

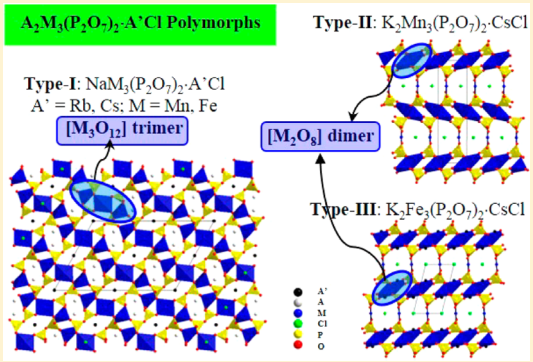

INTRODUCTION

"Although derivative-type synthesis plays an important role in developmental work, history also shows that synthetic discoveries that have led to landmark advances in solid state science have nearly always been made through exploratory synthesis rather than by design."[1] John D. Corbett (1926−2013). Countless new materials have been discovered, and the legacy of Corbett continues in the materials discovery world with endless surprises and amazements.

We have been interested in the exploratory synthesis and crystal growth of mixed-metal oxides in molten alkali and alkaline-earth metal halides as a high-temperature solvent. Occasional inclusion of halide salts was first thought to be inevitable. With the systematic selection of chemical systems and reaction conditions, the discoveries of a fascinating class of hybrid solids that are now known as salt-inclusion solids (SISs) have been made possible by employing halide salts as a reactive flux.[2] These newly emerged solids display an integrated structure between chemically dissimilar lattices of covalent metal oxide and ionic halide salt. Although the structure formation could be thought of as a result of "phase segregation" (for the lack of a better term) between covalent oxide lattices and space-filling and charge-compensating salts, it has been evident that the incorporated salts play an essential role in special framework formation and its unique chemical/physical properties. Systematic studies have shown that the salt lattices of SISs act as a template to the formation of covalent frameworks featuring micropores,[3] noncentrosymmetric lattices,[2,4] magnetic nanostructures,[5] and, better yet, mesopores[6] and water-soluble polyoxovanadate anions.[7] It should be noted that the formation of SISs has reportedly been observed in salt solutions under hydrothermal conditions showing the template nature of SIS formation.[8]

Among all of the SISs discovered thus far, the open frameworks of the $M_{2n-1}(X_2O_7)_n^{2-}$ (n = 1−4) type (M = divalent, first-row transition-metal (TM) cations; X = Si, P, As) have demonstrated the richest structural chemistry.[3,4c−e] These otherwise three-dimensional, mixed MO_x/XO_4 framework structures possess micropores with 8-ring (n = 1), mixed 8/16- and 24-ring (n = 2), 16-ring (n = 3), and 20-ring (n = 4) windows. Prior examples have shown that the shape and

Special Issue: To Honor the Memory of Prof. John D. Corbett

Received: October 9, 2014
Published: November 21, 2014

   dx.doi.org/10.1021/ic5024696 | Inorg. Chem. 2015, 54, 1136−1144

Table 1. Crystallographic Data for 1−6

	1	2	3	4	5	6
fw	727.04	679.60	729.76	682.32	759.27	761.98
cryst dimens, mm	0.20 × 0.18 × 0.16	0.21 × 0.18 × 0.15	0.18 × 0.15 × 0.12	0.16 × 0.14 × 0.10	0.18 × 0.12 × 0.10	0.16 × 0.12 × 0.08
cryst color, shape	light pink, column	light pink, column	light brown, column	light brown, column	light pink, column	light brown, column
space group, Z	$C2/c$ (No. 15), 4	$C2/c$ (No. 15), 4	$C2/c$ (No. 15), 4	$C2/c$ (No. 15), 4	$P2/c$ (No. 13), 2	$P\bar{1}$ (No. 2), 1
T, K	293(2)	293(2)	293(2)	293(2)	293(2)	293(2)
a, Å	21.201(4)	21.152(4)	20.884(7)	20.827(4)	7.6288(15)	5.3125(11)
b, Å	5.2811(11)	5.2405(10)	5.228(7)	5.1920(10)	5.3699(11)	7.6130(15)
c, Å	13.913(3)	13.853(3)	13.76(2)	13.709(3)	18.995(4)	9.6697(19)
α, deg	90	90	90	90	90	79.41(3)
β, deg	119.07(3)	119.45(3)	118.44	118.82(3)	100.92(3)	76.04(3)
γ, deg	90	90	90	90	90	89.66(3)
V, Å^3	1361.5(5)	1337.2(6)	1321(3)	1298.8(4)	764.1(3)	372.76(13)
d_{calcd}, g/cm^3	3.547	3.376	3.669	3.49	3.30	3.395
μ(Mo Kα), mm^{-1}	6.183	7.229	6.799	7.877	5.997	6.525
F(000)	1364	1292	1376	1304	714	360
GOF on F^2	1.125	1.115	1.084	1.138	1.115	1.102
final R indices [$I > 2\sigma(I)$][a]	R1 = 0.0267, wR2 = 0.0676	R1 = 0.0306, wR2 = 0.0752	R1 = 0.0235, wR2 = 0.0627	R1 = 0.0317, wR2 = 0.0779	R1 = 0.0304, wR2 = 0.0787	R1 = 0.0433, wR2 = 0.1138
R indices (all data)	R1 = 0.0275, wR2 = 0.0685	R1 = 0.0321, wR2 = 0.0771	R1 = 0.0241, wR2 = 0.0633	R1 = 0.0330, wR2 = 0.0793	R1 = 0.0313, wR2 = 0.0796	R1 = 0.0443, wR2 = 0.1147

[a] $R1 = \sum||F_o| - |F_c||/\sum|F_o|$; $wR2 = \{\sum[(F_o)^2 - (F_c)^2]^2/\sum w[(F_o)^2]^2\}^{1/2}$.

geometry of the pore windows can be varied by altering the identity and relative concentration of the incorporated salt.[3c,4e] However, there has never been a case where the resulting porous frameworks of the $M_{2n-1}(X_2O_7)_n^{2-}$ type contain anything other than M−O−X oxy linkages via the sharing of vertex O atoms of MO_x (x = 4 and 5) and $[X_2O_7]$ polyhedral units. This, of course, could be attributed to the M/X ratios being smaller than 1. When the M/X ratios are increased (≥1), the covalent frameworks begin to show the incorporation of multinuclear TM oxide units and, in addition to the oxy linkages, the formation of oxo, M−O−M, linkages.[5−7] To our pleasant surprise, mixed oxy/oxo linkages were found in the $M_3(P_2O_7)_2^{2-}$ family (n = 2), where the M/P ratio is less than 1 and it is intuitively anticipated for the network to be dominated by the formation of M−O−P bonds.

The open frameworks in the new series of the $M_3(P_2O_7)_2^{2-}$ type, as realized for the first time, exhibit M−O−M oxo linkages owing to the formation of dimeric $[M_2O_8]$ and trimeric $[M_3O_{12}]$ units as discussed later. These multinuclear TM oxide units can act as charge reservoirs of catalytic (with respect to redox catalysis) and magnetic interests owing to inherent multioxidation state of TM cations and superexchange pathways via the M−O−M bonds and super superexchange via the M−O −P−O−M linkages. Our new findings provide additional evidence to the well-recognized structural versatility of the mixed MO_x/XO_4 oxides related to, in particular, the $M_3(P_2O_7)_2^{2-}$-type open frameworks. Further, the frameworks described herein provide insight into the reticular chemistry of mixed-framework solids templated by ionic salts.

In this report, we illustrate the salt-inclusion synthesis of a new family of SISs adopting the general formula $A_2M_3(P_2O_7)_2$·A′Cl. The series includes six new compounds forming in three types of polymorphic structures, namely, type I, $Na_2Mn_3(P_2O_7)_2$·CsCl (**1**), $Na_2Mn_3(P_2O_7)_2$·RbCl (**2**), $Na_2Fe_3(P_2O_7)_2$·CsCl (**3**), and $Na_2Fe_3(P_2O_7)_2$·RbCl (**4**), type II, $K_2Mn_3(P_2O_7)_2$·CsCl (**5**), and type III, $K_2Fe_3(P_2O_7)_2$·CsCl (**6**). These new compounds contain trimeric (type I) and dimeric (types II and III) TM oxide units. **2** and **4** were subject to magnetic susceptibility studies showing bulk antiferromagnetic (AFM) properties, as expected. IR spectroscopy and differential scanning calorimetry (DSC) of **2** and **6** provide further information concerning the local structure and thermal stability of these SISs.

EXPERIMENTAL SECTION

All reactions were loaded in a nitrogen-purged drybox unless otherwise noted. The reactants and salts were first weighed and intimately ground with an agate mortar and pestle. The mixtures were placed in a silica ampule followed by flame sealing in air under vacuum. All chemicals were used as received: phosphorus oxide (P_4O_{10}; Aldrich, 98%), MnO (Alfa Aesar, 99.5%), FeO (Alfa Aesar, 99.9%), CsCl (Alfa Aesar, 99.99%), RbCl (Alfa Aesar, 99.8%), KCl (Alfa Aesar, 99.9%), and NaCl (Alfa Aesar, 99.9%).

Synthesis. Crystal growth of the title series was carried out in molten-salt media. The reactions employed 0.25−0.29 g of binary oxides and 1.8−2.3× by weight of alkali-metal chloride. Crystals of **2**, for instance, were acquired from the reaction containing 1.6 mmol (0.1135 g) of MnO and 0.50 mmol (0.1420 g) of P_4O_{10} and a eutectic salt (mp ∼540 °C) of 3.47 mmol (0.4192 g) of RbCl and 3.20 mmol (0.1870 g) of NaCl. (See Table S1 in the Supporting Information for the complete list of reactions.) The mixtures were heated to 750 °C at a rate of 3 °C/min, held for 12 h, slowly cooled, at a rate of 0.1 °C/min, to 350 °C, and then furnace-cooled to room temperature. After the products were washed with water to remove excess salt flux, the crystals of **1**−**6** were retrieved by a suction filtration method. Figure S1 in the SI shows the columnlike and irregular-shaped morphologies of as-grown clear crystals of **2** typical of the title compounds. The yield varied by ca. 30−50% in addition to unidentified powders.

After structure determination, a stoichiometric-yield synthesis was carried out according to the determined chemical composition. Attempts were made employing conventional high-temperature, solid-state reactions. For the Mn-containing phases, **1**, **2**, and **5**, stoichiometric amounts of the respective precursors A_2CO_3 (A = Na, K), $MnCO_3$ and $(NH_4)_2HPO_4$, along with the CsCl or RbCl salt, were mixed and ground in air. The mixtures were packed into a fused-silica ampule and heated slowly in two stages, i.e., at 300 °C for 2 h followed by 500 °C for 3 h, to avoid sudden decomposition of $(NH_4)_2HPO_4$. The latter releases gaseous NH_3 and H_2O products that may give rise to inhomogeneous mixing of the reactants. Intermittent grinding was employed before the reactions were reheated to 600 °C for 10 h for

dx.doi.org/10.1021/ic5024696 | Inorg. Chem. 2015, 54, 1136−1144

Table 2. Bond Distances (Å) and Bond Angles (deg) for the $[M_3O_{12}Cl]$ Unit in 2 and the $[M_2O_8]$ and MO_4Cl_2 Units in 5 and 6

Type I: $Na_2Mn_3(P_2O_7)_2$·RbCl (2)			
$Mn(1)O_5Cl$			
Mn(1)−O(3)	2.209(3)	Mn(1)−O(6)	2.172(4)
Mn(1)−O(4)	2.210(6)	Mn(1)−O(7)	2.104(34)
Mn(1)−O(5)	2.144(2)	Mn(1)−Cl	2.919(39)
$Mn(2)O_4Cl_2$			
Mn(2)−O(1) (×2)	2.028(16)	O(7)−Mn(1)−O(6)	93.89(9)
Mn(2)−O(4) (×2)	2.303(53)	O(1)−Mn(2)−O(4) (×2)	85.49(9)
Mn(2)−Cl	2.567(1)	O(1)−Mn(2)−O(4) (×2)	97.00(9)
Mn(2)−Cl	2.674(1)	O(1)−Mn(2)−O(1)	165.92(10)
O(3)−Mn(1)−O(4)	84.50(8)	O(4)−Mn(2)−O(4)	159.75(7)
O(4)−Mn(1)−O(5)	94.18(8)	Cl−Mn(2)−O(4) (×2)	100.12(5)
O(5)−Mn(1)−O(6)	101.95(8)	Cl−Mn(2)−O(1) (×2)	82.96(6)
O(6)−Mn(1)−O(7)	93.89(9)	Cl−Mn(2)−O(1) (×2)	97.04(6)
O(7)−Mn(1)−O(3)	84.03(9)	Cl−Mn(2)−O(4) (×2)	79.88(5)
O(7)−Mn(1)−O(4)	99.05(9)	Mn(1)−O(4)−Mn(2)	109.59(9)
O(7)−Mn(1)−O(5)	96.08(9)		
Type II: $K_2Mn_3(P_2O_7)_2$·CsCl (5)			
$Mn(1)O_5$			
Mn(1)−O(1)	2.091(5)	O(6)−Mn(1)−O(4)	117.19(9)
Mn(1)−O(2)	2.058(8)	O(6)−Mn(1)−O(4)	84.48(8)
Mn(1)−O(4)	2.098(4)	O(6)−Mn(1)−O(1)	89.66(9)
Mn(1)−O(4)	2.345(10)	O(2)−Mn(1)−O(4)	100.44(9)
Mn(1)−O(6)	2.080(24)	O(2)−Mn(1)−O(4)	85.27(8)
O(1)−Mn(1)−O(4)	115.83(9)	O(2)−Mn(1)−O(1)	88.07(9)
O(1)−Mn(1)−O(4)	162.00(9)	O(2)−Mn(1)−O(6)	138.96(9)
O(4)−Mn(1)−O(4)	81.88(8)	Mn(1)−O(4)−Mn(1)	98.12(9)
$Mn(2)O_4Cl_2$			
Mn(2)−O(3) (×2)	2.143(16)	Cl−Mn(2)−O(3) (×2)	87.58(6)
Mn(2)−O(5) (×2)	2.144(31)	Cl−Mn(2)−O(5) (×2)	93.31(7)
Mn(2)−Cl	2.679(1)	Cl−Mn(2)−O(3) (×2)	92.42(6)
Mn(2)−Cl	2.691(1)	Cl−Mn(2)−O(5) (×2)	86.69(7)
O(3)−Mn(2)−O(5) (×2)	93.96(9)	Cl−Mn(2)−Cl	179.99(3)
O(5)−Mn(2)−O(3) (×2)	86.32(9)		
Type III: $K_2Fe_3(P_2O_7)_2$·CsCl (6)			
$Fe(1)O_5$			
Fe(1)−O(2)	1.994(31)	O(4)−Fe(1)−O(2)	87.74(18)
Fe(1)−O(4)	2.067(30)	O(4)−Fe(1)−O(6)	90.91(19)
Fe(1)−O(5)	2.069(7)	O(4)−Fe(1)−O(5)	115.78(19)
Fe(1)−O(5)	2.315(38)	O(5)−Fe(1)−O(2)	86.95(17)
Fe(1)−O(6)	2.002(34)	O(5)−Fe(1)−O(6)	85.75(18)
O(2)−Fe(1)−O(6)	143.15(19)	O(5)−Fe(1)−O(5)	77.67(17)
O(6)−Fe(1)−O(5)	114.39(19)	Fe(1)−O(5)−Fe(1)	102.33(19)
O(5)−Fe(1)−O(2)	99.13(19)		
$Fe(2)O_4Cl_2$			
Fe(2)−O(3) (×2)	2.072(21)	Cl−Fe(2)−O(3) (×2)	88.45(14)
Fe(2)−O(7) (×2)	2.118(36)	Cl−Fe(2)−O(7) (×2)	94.03(15)
Fe(2)−Cl (×2)	2.656(1)	Cl−Fe(2)−O(3) (×2)	91.55(14)
O(3)−Fe(2)−O(7) (×2)	85.73(18)	O(7)−Fe(2)−O(7) (×2)	180.00(19)
O(7)−Fe(2)−O(3) (×2)	94.27(18)	Cl−Fe(2)−Cl	180.00(2)
Cl−Fe(2)−O(7) (×2)	85.97(15)		

decomposition of the carbonate precursors. The mixtures were then reground, followed by reheating at 620 °C for 2 days.

For the Fe-based phases, **3**, **4**, and **6**, reaction mixtures were carried out in a closed container by sealing in a fused-silica ampule under vacuum to avoid the apparent oxidation of Fe^{2+} to Fe^{3+} in air. Stoichiometric amounts of analytical-grade A_2CO_3 (A = Na, K), FeO, P_4O_{10}, and CsCl/RbCl were weighed and ground in the nitrogen-purged drybox. It is noted that the reactions were sealed in longer tubes in order to reduce the potential pressure buildup, which can break the ampule because of the volatile CO_2 gas yielded from decomposition of the carbonate precursors. A good portion of the reaction ampule was placed in the cooler region near the top of the furnace where the 0.5 in. opening window is. Nevertheless, the mixtures were heated to 600 °C at a rate of 0.5 °C/min, held for 2 days, and then slowly cooled to room temperature.

The as-prepared polycrystalline samples were subjected to the powder X-ray diffraction (PXRD) studies. Figure S2 in the SI shows the observed and, for comparison, calculated patterns. The results regarding phase formation are presented later in the Results and Discussion section.

Crystallographic Studies. Crystals of **1**−**6** were selected under an optical microscope equipped with a polarizing light attachment. The

dx.doi.org/10.1021/ic5024696 | Inorg. Chem. 2015, 54, 1136−1144

Table 3. Refined Cell Parameters of 1−6

	1	2	3	4	5	6
a, Å	21.194(2)	21.159(1)	20.888(4)	20.822(7)	7.623(6)	5.311(4)
b, Å	5.278(2)	5.241(2)	5.230(6)	5.191(6)	5.369(5)	7.617(6)
c, Å	13.906(2)	13.852(2)	13.756(7)	13.699(7)	18.970(8)	9.655(5)
α, deg						79.4(3)
β, deg	119.06(1)	119.47(3)	118.43(4)	118.81(5)	100.92(9)	76.0(3)
γ, deg						89.6(3)
V, Å^3	1359.7(4)	1337.4(5)	1321.6(6)	1297.4(3)	762.3(3)	372.2(5)

data crystal was mounted on a glass fiber with epoxy for X-ray diffraction studies. The data were collected at room temperature on a Rigaku AFC8 diffractometer equipped with a Mercury CCD area detector with Mo Kα (λ = 0.71073 Å) radiation. An empirical multiscan absorption correction was applied using *REQAB*, a subroutine of the *CrystalClear* software package.[9] The structure was solved by direct methods using the *SHELEX-97* program and refined on F^2 by full-matrix least-squares techniques.[10] The final results were examined by *PLATON*, and no additional symmetry was suggested. Table 1 reports the crystallographic data of **1**−**6** and Table 2 the selected bond distances and angles of **2**, **5**, and **6**.

PXRD. The PXRD data were collected using a Rigaku Ultima IV diffractometer equipped with Cu Kα radiation (λ = 1.5406 Å) and a graphite monochromator. Each pattern was collected in the range of 5−55° with a scan speed of 0.1 s and a step size of 0.02° in 2θ. *PDXL* software[11] provided by Rigaku was used for further data analysis. Powder X-ray refinements were done using the *Fullprof* software package[12] on polycrystalline powder samples. The peak positions, background, scale factor, and profile parameters were refined individually until convergence was achieved. The unit cell and zero shift were refined simultaneously until convergence was reached.

IR Spectroscopy. IR spectroscopy was carried out using a Nicolet IR 200 spectrometer in the range of 4000−400 cm^{-1}. Samples were prepared using approximately a 1:100 (by mass) mixture of selected crystals of **2** or **6** with spectral-grade KBr. The mixture was ground and pressed into a pellet under 10000 psi.

DSC. DSC measurements on a ground powder of selected crystals of **2** (∼10.1 mg) and **6** (∼2.0 mg) were done using a SDT Q600 TA Instruments calorimeter. The heating profile for the measurement included a heating rate of 15 °C/min from room temperature to 800 °C, followed by a return cooling rate of 15 °C/min under a 75 mL/min nitrogen gas flow.

Magnetic Measurements. The temperature dependence of the magnetic susceptibility was measured with a Quantum Design SQUID (superconducting quantum interference device) MPMS7T magnetometer. A ground polycrystalline sample of selected single crystals of **2** (6.3 mg) and **4** (17.1 mg) was placed in a gel capsule. The initial studies were performed over 2−300 K in an applied field of 500 Oe. The magnetic susceptibility was corrected for the contribution of the gel capsule and for the core diamagnetism (using Pascal Ms constants).

RESULTS AND DISCUSSION

Synthesis. The crystals of **2** were initially formed serendipitously in reactions where Mn/P > 1 and were intended to explore new TM oxo compounds similar to the recently discovered manganese(III) germanate, $KMn_3O_2(Ge_2O_7)$, which contains pillared $[Mn_3O_8]_\infty$ (S = 2) magnetic kagome sheets.[13] The reaction was set up to explore compound formation in the Mn-rich region of the $MnO-P_4O_{10}$ binary phase diagram and P^V was substituted for Ge^{IV} with the hope of isolating the $S = {}^5/_2$ kagome sheet. While no compound with an extended $[Mn^{II}{}_3O_8]_\infty$ kagome sheet was identified, a new member of the title series, $Na_2Mn_3(P_2O_7)_2$·CsCl, was isolated in low yield.

The chemical compositions of the six new phases adopt the general formula $A_2M_3(P_2O_7)_2$·A′Cl, where the radius $r(A^+) < r(A'^+)$. The reaction mixtures employed the corresponding TM monoxides (MO) and P_4O_{10} for crystal growth, along with alkali-metal chloride (A′Cl) salts. The source of the A-site cation was presumably provided in situ via the metathesis reaction involving one of the eutectic chloride salts that adopts a smaller alkali-metal cation, e.g., $2ACl + MO \rightarrow A_2O + MCl_2$. The reaction generates alkali-metal oxides (A_2O; A = Na, K), which are otherwise commercially unavailable. Although no reaction mechanism has been known concerning the incorporation of chloride salts, one can imagine that metal oxides are first "dissolved" in the "corrosive" molten-salt media and then, upon cooling, the covalent lattice aggregates within and/or around the inherent structures of molten ionic lattices. The reaction temperatures were arbitrarily determined but practically set high enough to facilitate a window of the molten state for crystal growth upon cooling.

The title compounds can be prepared in polycrystalline samples at lower temperatures. Attempts were made using carbonates of the respective cations (A_2CO_3; A = Na, K) and/or dibasic ammonium phosphate [$(NH_4)_2HPO_4$] precursors. The reaction temperatures were set at 600−620 °C, which is significantly lower than 750 °C for crystal growth and below the decomposition temperature (vide infra). PXRD analysis of as-prepared polycrystalline samples (Supporting Information, Figure S2) indicates that **1**−**6** were formed in the respective polymorphs, suggesting that the polymorphic structures are dictated likely by the size of the A-site cations discussed below. Of course, one cannot rule out the possibility of the coexistence of multiple polymorphs. Nevertheless, the refined cell parameters, as shown in Table 3, are comparable with those of PXRD in Table 1.

Structure Description. The six compounds adopt three types of polymorphic structures. For the purpose of structure illustration, **2** is discussed as a representative member of the type I polymorphs **1**−**4** of isostructure $Na_2M_3(P_2O_7)_2$·A′Cl (M = Mn, Fe; A′ = Rb, Cs), while **5** and **6** are illustrated respectively for types II and III.

2 crystallizes in a monoclinic crystal system ($C2/c$, No. 15). As shown in Figure 1, the extended structure of **2** exhibits channels and $[Mn_3O_{12}]$ trimeric units. Plots of projected views along the *b* (Figure 1a) and *c* (Figure 1b) axes reveal two types of channels, where the respective Na^+ cations and RbCl salt lattice reside. The framework structure is constructed by the interlinked $[Mn_3O_{12}]$ trimeric units via Mn−Cl−Mn bonds along *b*, as shown in Figure 1c. It shows two neighboring $[Mn_3O_{12}Cl]_\infty$ chains being interconnected by the $[P_2O_7]$ pyrophosphate units via the sharing of bridging O atoms, O(4), of the trimer. The $[Mn_3O_{12}]$ trimeric units are made of corner-shared polyhedra $Mn(1)O_5-Mn(2)O_4-Mn(1)O_5$ (Figure 1d) with the square planes of the two outer units facing toward the

dx.doi.org/10.1021/ic5024696 | Inorg. Chem. 2015, 54, 1136−1144

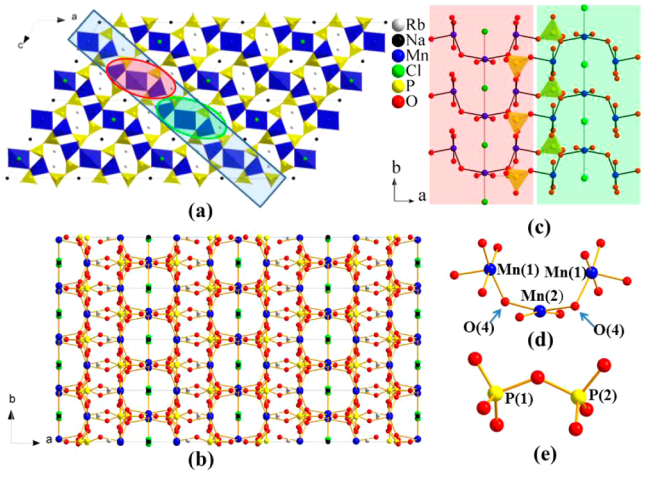

Figure 1. Structure of **2**, a type I polymorph, showing the channels along the (a) *b* and (b) *c* axes that are made of (c and d) $[Mn_3O_{12}]$ trimeric building units and (e) P_2O_7. The antiparallel arrangement of neighboring trimers is highlighted in pink and green bands; see the text.

Cl atom to form long Mn(1)···Cl interactions (not shown for clarity), e.g., 2.919(39) Å, and a curved structure. The stacked $[Mn_3O_{12}]$ trimeric units shown in Figure 1c are concave upward in one array (highlighted in pink) and downward in another (in green), alternately progressing along the slab highlighted with a light-blue band in Figure 1a.

The channels of the type I polymorph exhibit 6-membered-ring windows made of alternating edges of $2P_2O_7$ and $2Mn(2)O_4$ polyhedra around A′ (=Rb) and $2P_2O_7$ and $2Mn(1)O_5$ around A-site (=Na) cations. The channels centered by the Rb^+ cations are at the intersections of the (200) and (002) planes in Figure 1a. These A′-site cations form the linear A′−Cl ionic lattice along *c*, showing the template effect to the two crystallographically nonequivalent Mn cations of the $Mn_3(P_2O_7)_2^{2-}$ covalent lattice. In Figure 2b, each Cl^- anion forms the two long Mn(1)···Cl bonds (dotted lines) mentioned above along *a* and two short Mn(2)−Cl bonds along *b*, e.g., 2.567(1) and 2.674(1) Å (see Table 2). The latter is comparable with 2.61 Å, the sum of Ahrens ionic radii of six-coordinate Mn^{II}, 0.80 Å, and Cl^-, 1.81 Å.[14] This longer Mn···Cl distance is similarly found in the previously reported *α*- and *β*-$Cs_3KBi_2Mn_4(PO_4)_6Cl$, e.g., 2.91 Å.[4a]

The two crystallographically distinct Mn^{II} sites are octahedrally coordinated by O and Cl atoms in the $Mn(1)O_5Cl$ and $Mn(2)O_4Cl_2$ units. As shown in Table 2, the average Mn−O distances are 2.168 and 2.166 Å, respectively, which are comparable with the sum of Shannon crystal radii, 2.18 Å, of a six-coordinate Mn^{II} cation, 0.96 Å (high spin, HS), and O^{2-}, 1.22 Å. The formal oxidation state of Mn^{2+} is further supported by the calculated bond-valence-sum (BVS) values (see the Supporting Information, Table S2).[15] A successful stoichiometric yield synthesis further confirms the chemical composition and oxidation states of the title compound (see the PXRD pattern in the Supporting Information, Figure S2).

Attempts to synthesize the A = K derivative of **1**−**4** led to the discoveries of two new CsCl-containing compounds of polymorphic type II, **5**, and type III, **6**. **5** crystallizes in a monoclinic crystal system (*P*2/*c*, No. 13) and **6** in a triclinic system ($P\bar{1}$, No. 2). These two types of polymorphs are quite comparable regarding the formation of dimeric $[M_2O_8]$ building units and the channel morphologies, as shown in Figures 3 and S3 in the Supporting Information. The major difference lies in the stacking orientations of the $[M_2O_8]$ units, upon which the extended frameworks are formed; see Figures 4 and S4 in the Supporting Information.

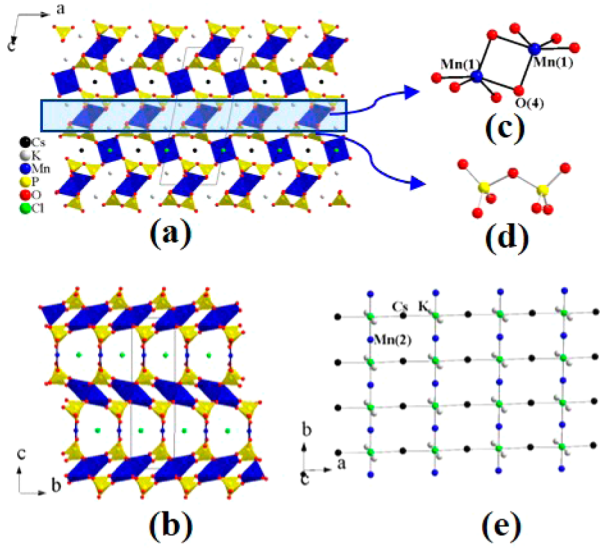

Figure 3. Structure of **5**, a type II polymorph, showing (a and b) the channels, (c) dimeric $[M_2O_8]$ and (d) P_2O_7 building units, and (e) a Mn−Cl−(Cs, K) sheet; see the text.

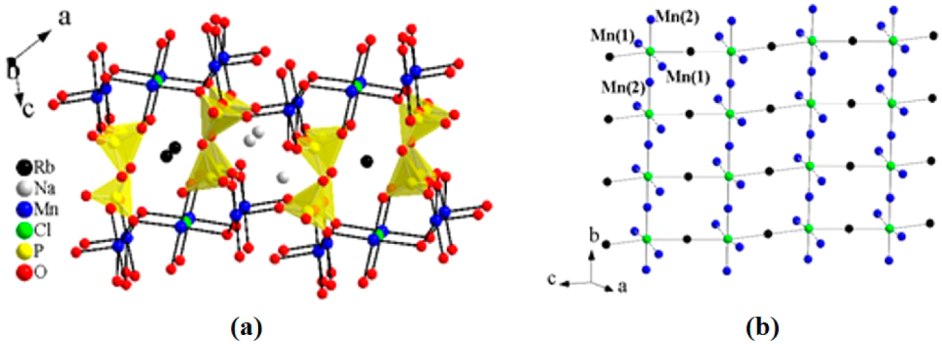

Figure 2. (a) Projected view showing the MnO_x (x = 4 and 5) and P_2O_7 units around the channels. (b) Slab of the Rb−Cl−Mn lattice showing the template effect of Cl atoms; see the text.

dx.doi.org/10.1021/ic5024696 | *Inorg. Chem.* 2015, 54, 1136−1144

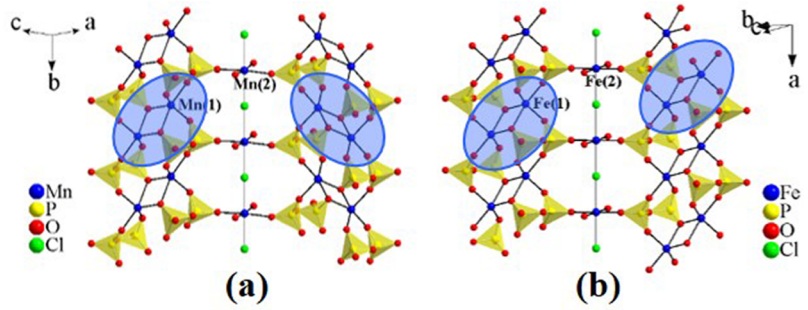

Figure 4. Partial structures of the type II and III $Mn_3(P_2O_7)_2^{2-}$ frameworks showing the arrangements of the $[M(1)_2O_8]$ dimers in (a) *monoclinic* **5** and (b) *triclinic* **6**. The shaded blue circles highlight the antiparallel and parallel orientations of the dimeric units in the respective structures; see the text.

In **5**, the multichannel structures, in which Cs^+ and K^+ ions reside, exhibit respective 6- and 8-membered-ring windows as viewed along *b* (Figure 3a). There are two additional channels as the structure is viewed along *a* where 4- and 8-membered-ring windows are shown (Figure 3b). The latter is centered by the linear CsCl chain. Different from the type I structure, the $Mn_3(P_2O_7)_2^{2-}$ covalent framework consists of the $[Mn(1)_2O_8]$ dimeric unit (Figure 3c). These dimers are interlinked through the P_2O_7 units (Figure 3d), with the $Mn(2)O_4Cl_2$ units extending into the lattice along the *ac* plane, as discussed in the later section. The Mn(2) ions serve as linkers connecting the aforementioned CsCl chains via the Mn−Cl bonds, e.g., 2.679(1) and 2.691(1) Å (Table 2), along *b*, as shown in Figure 3e, to form a sheet extending along the *ab* plane. Each Cl coordinates to additional Cs ions to form the $ClCs_2K_2Mn_2$ octahedral environment. All of these features are adopted by the structure of the type III polymorph, which will not be reiterated for simplicity.

The major difference between the structures of type II and III polymorphs lies in the relative orientations of the stacked $[M(1)_2O_8]$ units. As illustrated in Figures 4 and S4 in the Supporting Information, the $[M(1)_2O_8]$ units stack along *b* for type II and along *a* for type III and are interconnected by the P_2O_7 units via sharing of the vertex O atoms. The dimeric units in the neighboring stacks show antiparallel (herringbone-like) arrangements when M = Mn (type II) and parallel when M = Fe (type III). These neighboring stacks are interlinked by the $[M(2)O_4Cl_2]$ unit in such a way as to form 8-membered-ring channels; see Figures 3b and S4 in the Supporting Information. The shape of the respective channels is seemingly altered. The windows appear to be less symmetrical in **5** (shieldlike) than in **6** (diamondlike). The origin of different stacking and the formation of different polymorphs, however, is unclear.

The $[M_2O_8]$ dimers are constructed by two distorted $M(1)O_5$ polyhedral units that share a common edge. The M(1)−O distances are in the ranges of 2.080(24)−2.345(10) Å for M = Mn and 1.994(31)−2.315(38) Å for M = Fe; see Table 2. The average M−O distances are 2.134 Å (Mn−O) and 2.089 Å (Fe−O), which are respectively comparable with the sum of the Shannon crystal radii, 2.11 and 2.06 Å, of an estimated five-coordinate Mn^{II}/Fe^{II} cation, 0.89/0.84 Å, and O^{2-}, 1.22 Å.[14] The formal oxidation state of M^{2+} is further supported by the calculated BVS values, as shown in the Supporting Information, Table S2.[15] Like those of the type I polymorph, a successful stoichiometric yield synthesis further confirms the chemical compositions and oxidation states of these two phases (see the PXRD patterns in Figure S2 in the Supporting Information and the refined cell parameters in Table 3).

It is worth noting that Cl-centered units in **1**−**6** are varied to accommodate the overall porous framework formation. As shown in Figures 2b and 3e, the Cl atom is surrounded by four M, 2Mn(1,2), and two A′, Cs, atoms in **1**−**4** (Figure 2b) but two each of M (=Mn or Fe), Cs, and K atoms in **5** and **6** (Figure 3e). In **1**−**4**, the Na atom does not bond to the chloride lattice.

It is fascinating to realize that the title series $A_2M_3(X_2O_7)_2{\cdot}A'Cl$ confirms the assertion that the incorporated ionic lattice dictates and templates formation of the $Mn_3(P_2O_7)_2^{2-}$ covalent framework. Compared to the formulas $A_2M_3(X_2O_7)_2{\cdot}3CsCl$ and $A_2M_3(X_2O_7)_2{\cdot}2CsCl$ (A = Na, K, Rb, Cs; M = Mn, Cu; X = P, As) of the previously reported porous compounds of the kind,[3b,c] it appears to be that, as the A′Cl salt concentration decreases, the open framework begins to condense by way of formation of the multinuclear TM oxide units and thus the M−O−M oxo linkages. When the size of the A-site cation is reduced, higher nuclearity in the multinuclear TM oxide units is observed. More specifically, the size of the TM oxide units increases from dimeric to trimeric as the A-site cation is changed from bigger K^+ (in types II and III) to smaller Na^+ (type I) cations.

While the salt in $A_2M_3(X_2O_7)_2{\cdot}3CsCl$ compounds can be removed by washing with water at room temperature and $A_2M_3(X_2O_7)_2{\cdot}2CsCl$ exchanged at elevated temperatures, the ionic lattices in the title compounds $A_2M_3(X_2O_7)_2{\cdot}A'Cl$ can be neither washed nor ion-exchanged. The main reason is that the channels in the title series are relatively small and the chloride ions are bonded to TM cations fairly strongly, as is evident in comparably short M−Cl distances. This big structural difference is apparently mainly due to the varied amount of salts in these structures. $A_2M_3(X_2O_7)_2{\cdot}3CsCl$ contains 3 mol of CsCl and produces a 12.7 Å diameter micropore. $A_2M_3(X_2O_7)_2{\cdot}2CsCl$ contains 2 mol of CsCl and possesses 4.9 Å × 17.2 Å elliptical channels. The title compounds contain 1 mol of A′Cl (A′ = Rb, Cs), and the size of the maximum dimension of the channels is below 6.0 Å. In $A_2M_3(X_2O_7)_2{\cdot}mCsCl$ ($m > 1$), the porous framework is made of only M−O−X oxy linkages; namely, MO_x ($x = 4$−6) polyhedra are isolated with each other. These indicate that the more salt present, the more likely it can help formation of the microporous materials, and less salt leads to the formation of a TM oxide nanostructure of magnetic importance.

IR Studies. As shown in Figure 5, the IR spectra of **2** (type I) and **6** (type III) are similar, as expected because these two compounds contain the same $[P_2O_7]$ building units. The peaks at 716/905 cm^{-1} for **2** and at 749/902 cm^{-1} for **6** are attributed to symmetric (ν_s) versus asymmetric (ν_{as}) P−O−P vibrations.

dx.doi.org/10.1021/ic5024696 | *Inorg. Chem.* 2015, 54, 1136−1144

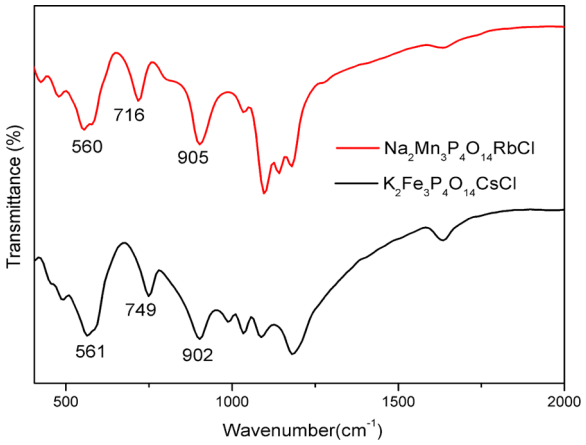

Figure 5. IR spectra of **2** (top) and **6** (bottom).

The difference in the P−O−P angles, 132.9(1) versus 123.8(3)°, respectively, may be responsible for the red shift. The O−P−O bending and P−O stretching vibrational frequencies associated with the PO_4 groups are shown as multiple bands in the ranges 400−680 and 1000−1300 cm^{-1}, respectively. These are similarly found in compounds containing $[P_2O_7]$ groups, such as $Na_2MnP_2O_7$, $NaCsMnP_2O_7$, and $K_2CuP_2O_7$.[16] The small differences usually come from the differences of the P−O−P and O−P−O angles.

Thermal Studies. The thermal properties of the title series were evaluated by DSC analysis. Because of the lack of a good sample for **5**, only some selected crystals of **2** and **6** were performed. As seen in Figure 6, there is one endothermic peak

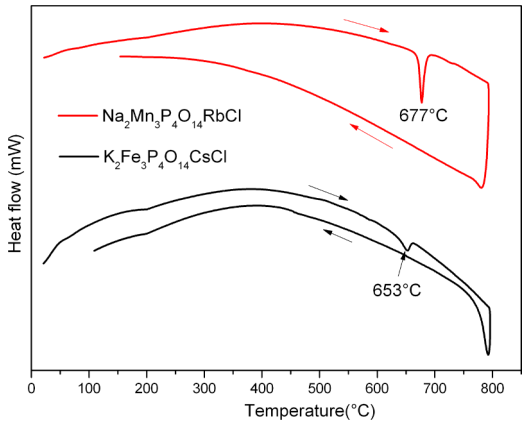

Figure 6. DSC curves of **2** (top) and **6** (bottom).

corresponding to the onset temperature of 677 °C for **2**. Because no melt was observed upon conclusion of the DSC measurement, the endothermic peak is believed to be associated with decomposition. The DSC curve of **6** (red line in Figure 6) also shows similar features. The decomposition temperature is 653 °C and is lower than that of **2**. This suggests that **2** and **6**, and likely other members of the series, are thermally stable up to 650 °C; thus, the stoichiometric-yield synthesis temperatures were set below that.

Magnetic Studies. In light of the unusual magnetic properties associated with compounds containing confined (low-dimensional) multinuclear magnetic nanostructures, the title series was subjected to preliminary magnetic measurements. The temperature (T) dependence of the molar magnetic susceptibility (χ), the inverse molar magnetic susceptibility (χ^{-1}), and the product χT of **2** and **4**, as shown in Figures 7 and

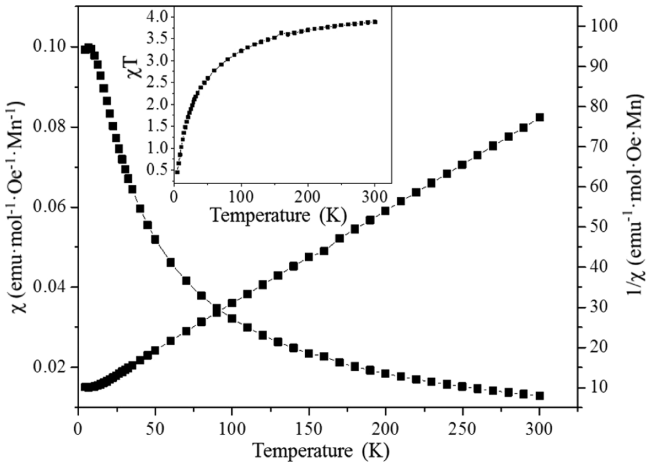

Figure 7. Magnetic susceptibility of **2**.

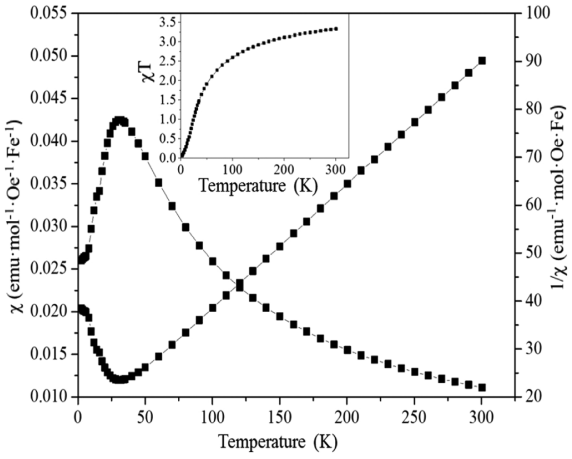

Figure 8. Magnetic susceptibility of **4**.

8, respectively, is taken in a small applied field (H = 500 Oe). **2** and **4**, as mentioned above, contain a trinuclear, 0D $[M_3O_{12}]$ unit and a 1D $[Mn_3O_{12}Cl]$ chain that are structurally isolated and electronically insulated by the closed-shell, nonmagnetic $[P_2O_7]$ groups. In Figure 7, the plot of χ^{-1} versus T was fitted with the Curie−Weiss law, $\chi = C/(T - \theta)$, at temperatures above T_N ~6 K, resulting in Curie constant C = 4.34 emu·K/mol and Weiss temperature θ = −33.88 K. The effective magnetic moment is calculated according to $\mu_{eff} = (8C)^{1/2}$ as 5.90 μ_B/Mn^{2+}, which is in good agreement with the spin-only value of 5.92 μ_B/Mn^{2+}. The negative Weiss constant suggests that spin interactions in **2** are predominantly AFM. As shown in the inset, the continuous decrease in the χT values when the temperature decreases is possibly attributed to intratrimer AFM spin coupling consistent with the nonorthogonal ∠Mn(1)−O(4)−Mn(2) angle, 109.59(9)°, as listed in Table 2. This is typical in compounds containing multinuclear TM oxide units of the kind.[17]

The intracluster AFM coupling is similarly observed in **4**, which is one of the other isostructural compounds adopting the type I polymorph. The molar susceptibility increases with

dx.doi.org/10.1021/ic5024696 | Inorg. Chem. 2015, 54, 1136−1144

decreasing temperature, showing a relatively broad peak appearing at ~32 K (T_N). This is expected of a low-dimensional antiferromagnet. The plot of χ^{-1} versus T was fitted with the Curie–Weiss law at temperatures between 50 and 300 K, resulting in Curie constant C = 3.89 emu·K/mol and negative Weiss temperature θ = −50.22 K. This negative θ value indicates that predominant magnetic interactions between Fe^{2+} ions are AFM. The effective magnetic moment is calculated to be 5.58 μ_B/Fe^{2+}, which is bigger than the anticipated spin-only value of 4.9 μ_B/Fe^{2+}, indicating a possible orbital contribution of the Fe^{2+} d^6 magnetic ions. In fact, the effective magnetic moment is comparable with the expected value 5.48 μ_B/Fe^{2+}, taking into account the orbital contribution (L = 2) of high-spin (S = 2) Fe^{2+} ions in the oxide environment.

Looking at the χT versus T plot in Figure 8 (inset), one can capture a change of the slope toward low temperatures. The magnetic susceptibility shows a corresponding kink at ~18 K, indicating the possible existence of additional intertrimer ferromagnetic interaction via possibly the Mn(2)–Cl–Mn(2) bonds in the 1D $[Mn_3O_{12}Cl]$ chain and/or the trimers of neighboring chains. Further magnetic studies are in order.

Final Remarks. The extended utility of salt-inclusion chemistry once again has revealed its role in exploring new special frameworks, in particular polymorphic SISs exhibiting multinuclear TM oxide units in salt-templated microporous frameworks. It is known that molten-salt flux can serve dual purposes. The salt, on the one hand, acts as a high-temperature solvent for the growth of otherwise refractory oxides and, on the other hand, interacts as a reactive agent for the formation of new SISs upon the manipulation of the salt content. The title series, in fact, is a new family of the $M_3(X_2O_7)_2^{2-}$-type derivatives that exhibit an already rich structural chemistry.

The six new solids serendipitously discovered in the reduced amount of molten chloride salts adopt the general formula $A_2M_3(P_2O_7)_2{\cdot}A'Cl$ and form three polymorphs. **1**–**4** adopt type I polymorphs having A/A′ = Na/(Rb,Cs) and M = Mn, Fe (**5**), type II with A/A′ = K/Cs and M = Mn (**6**), and type III with A/A′ = K/Cs and M = Fe. In these reactions, 1.8–2.3×, as opposed to normally 3×, by weight of alkali-metal chloride was employed. Compared with the structures of the previously reported $A_2M_3(X_2O_7)_2{\cdot}n$CsCl (n = 2 and 3) families, it becomes apparent that incorporating a lesser amount of the A′Cl salt (n = 1), along with a smaller A-site cation, $r(A^+) < r(A'^+)$, is responsible for the formation of multinuclear TM oxide units.

This discovery suggests that it is possible to incorporate multinuclear units without increasing the M/X ratios, as realized for the first time, but adjusting the content of the ionic lattices. In the $M_3(X_2O_7)_2^{2-}$-type frameworks that are otherwise well-known for their sole existence of isolated mononuclear MO_x units and M–O–X oxy linkages, there are now polymorphic compounds containing TM oxide units of monomeric MO_x, dimeric $[M_2O_8]$, and trimeric $[M_3O_{12}]$ for systematic magnetic studies. For the future effort of the so-called designed synthesis, this study seems to indicate that, through substitution of a bigger A-site cation, $r(K^+) > r(Na^+)$, a larger pore can be created by reducing the size of the multinuclear units (such as from trimeric units in the type I polymorph of the Na-based derivatives to dimeric in types II and III of the K-based derivatives).

It is amazing to see that the two K derivatives, $K_2M_3(P_2O_7)_2{\cdot}$CsCl, adopt two closely related but different polymorphs (monoclinic vs triclinic). The difference seemingly depends upon the M = Mn (type II) and Fe (type III) polymorphs that result in frameworks containing antiparallel versus parallel stacking of the corresponding $[M_2O_8]$ units. The origin of the difference, however, is yet to be identified.

These compounds are stable up to 650 °C in nitrogen. Magnetic studies of the selected compounds in the series suggest, as expected, bulk AFM properties.

Last but not the least, strategically employing a "balanced" amount of chloride salt, one can incorporate multinuclear TM oxide units even with the M/P < 1 necessary for the confinement effect. The current finding is of fundamental importance relevant to the systematic study of the size-dependent magnetic behavior of multinuclear TM oxide units that are "imbedded" in the comparable oxide matrix made of closed-shell, nonmagnetic insulating oxyanions. The study also provides insight into reticular chemistry with regard to the formation of desired mixed-framework solids by altering the identity and concentration of the ionic salt.

■ ASSOCIATED CONTENT

Ⓢ Supporting Information

X-ray crystallographic file in CIF format, PXRD patterns, structure drawings of the packing of multinuclear units, and BVS calculations. This material is available free of charge via the Internet at http://pubs.acs.org.

■ AUTHOR INFORMATION

Corresponding Author

*E-mail: shwu@clemson.edu

Author Contributions

‡The manuscript was written through contributions of all authors. All authors have given approval to the final version of the manuscript. These authors contributed equally.

Notes

The authors declare no competing financial interest.

■ ACKNOWLEDGMENTS

This work has been supported by the National Science Foundation (NSF; Grant DMR-0706426). Support for the purchase of a SQUID magnetometer (Grant CHE-9808044) and an X-ray diffractometer (Grants ESR-9108772, CHE-9207230, and 9808165) from the NSF is acknowledged. Also acknowledged is support by the National Natural Science Foundation of China (Grant 51002119) for this work and China Scholarship Council for an academic visit (J.G.) at Clemson University.

■ REFERENCES

(1) Corbett, J. D. *Pure Appl. Chem.* **1984**, *56*, 1527–1543.

(2) West, J. P.; Hwu, S.-J. *J. Solid State Chem.* **2012**, *195*, 101–107.

(3) (a) Huang, Q.; Ulutagay, M.; Mo, X.; Hwu, S.-J. *Mater. Res. Soc. Symp. Proc.* **2003**, *755*, 459–464. (b) Huang, Q.; Ulutagay, M.; Michener, P. A.; Hwu, S.-J. *J. Am. Chem. Soc.* **1999**, *121*, 10323–10326. (c) Hwu, S.-J.; Mo, X. *Angew. Chem., Int. Ed.* **2001**, *40*, 1690–1693.

(4) (a) West, J. P.; Sulejmanovic, D.; Hwu, S.-J.; He, J.; VanDerveer, D.; Johnson, B. K. *Inorg. Chem.* **2012**, *51*, 9723–9729. (b) Queen, W. L.; West, J. P.; Hwu, S.-J.; VanDerveer, D. G.; Zarzyczny, M. C.; Pavlick, R. A. *Angew. Chem., Int. Ed.* **2008**, *47*, 3791–3794. (c) Mo, X.; Ferguson, E.; Hwu, S.-J. *Inorg. Chem.* **2005**, *44*, 3121–3126. (d) Mo, X.; Hwu, S.-J. *Inorg. Chem.* **2003**, *42*, 3978–3980. (e) Huang, Q.; Hwu, S.-J. *Inorg. Chem.* **2003**, *42*, 655–657. (f) Etheredge, K. M. S.; Hwu, S.-J. *Inorg. Chem.* **1995**, *34*, 3123–3126.

(5) (a) Gnezdilov, V.; Bedarev, V.; Gnatchenko, S.; Pashchenko, M.; Pashkevich, Y.; Lemmens, P.; Zvyagin, S.; Mo, X.; Queen, W.; Hwu, S.-J. *Low Temp. Phys.* **2007**, *33*, 684−687. (b) Stern, R.; Heinmaa, I.; Kriisa, A.; Joon, E.; Vija, S.; Clayhold, J.; Ulutagay-Kartin, M.; Mo, X.; Queen, W.; Hwu, S.-J. *Phys. B: Condens. Matter* **2006**, *378*−*380*, 1124−1125. (c) Clayhold, J. A.; Ulutagay-Kartin, M.; Hwu, S.-J.; Koo, H.-J.; Whangbo, M.-H.; Voigt, A.; Eaiprasertsak, K. *Phys. Rev. B* **2002**, *66*, 052403/1−052403/4. (d) Hwu, S.-J.; Ulutagay-Kartin, M.; Clayhold, J. A.; Mackay, R.; Wardojo, T. A.; O'Connor, C. T.; Krawiec, M. *J. Am. Chem. Soc.* **2002**, *124*, 12404−12405. (e) Ulutagay, M.; Schimek, G. L.; Hwu, S.-J.; Taye, H. *Inorg. Chem.* **1998**, *37*, 1507−1512. (f) Etheredge, K. M. S.; Hwu, S.-J. *Inorg. Chem.* **1996**, *35*, 5278−5282.

(6) Queen, W. L.; Hwu, S.-J.; Reighard, S. *Inorg. Chem.* **2010**, *49*, 1316−1318.

(7) (a) Queen, W. L.; West, J. P.; Hwu, S.-J.; Tran, T. T.; Halasyamani, P. S.; VanDerveer, D. *Chem. Commun.* **2012**, *48*, 1665−1667. (b) Queen, W. L.; West, J. P.; Hudson, S.-J.; Hwu, S.-J. *Inorg. Chem.* **2011**, *50*, 11064−11068.

(8) For instance, see: (a) Yu, H.; Pan, S.; Wu, H.; Yang, Z.; Dong, K.; Su, X.; Zhang, B.; Li, H. *Cryst. Growth Des.* **2013**, *13*, 3514−3521. (b) Chang, Y.-C.; Chang, W.-J.; Boudin, S.; Lii, K.-H. *Inorg. Chem.* **2013**, *52*, 7230−7235. (c) Yu, H.; Wu, H.; Pan, S.; Wang, Y.; Yang, Z.; Su, X. *Inorg. Chem.* **2013**, *52*, 5359−5365.

(9) *CrystalClear*; Rigaku/MSC: The Woodlands, TX, 1999.

(10) (a) Sheldrick, G. M. In *Crystallographic Computing 3*; Sheldrick, G. M., Kruger, C., Goddard, R., Eds.; Oxford University Press: London, 1985; pp 175−189. (b) Sheldrick, G. M. *SHELXTL, Version 6.1, Structure Determination Software Programs*; Bruker Analytical X-ray Systems Inc.: Madison, WI, 2001.

(11) *Rigaku J.* **2010**, *26*, 23-27.

(12) Rodrigues-Carvajal, J. *Physica B* **1993**, *192*, 55−69.

(13) Williams, M. S.; West, J. P.; Hwu, S.-J. *Chem. Mater.* **2014**, *26*, 1502−1504.

(14) Shannon, R. D. *Acta Crystallogr.* **1976**, *A32*, 751−767.

(15) (a) *VALENCE for DOS*, version 2.0: Brown, I. D. *J. Appl. Crystallogr.* **1996**, *29*, 479−480. (b) Brown, I. D.; Altermatt, D. *Acta Crystallogr.* **1985**, *B41*, 244−247.

(16) (a) Huang, Q.; Hwu, S.-J. *Inorg. Chem.* **1998**, *37*, 5869−5874. (b) ElMaadi, A.; Boukhari, A.; Holt, E. M. *J. Alloys Compd.* **1995**, *223*, 13−17.

(17) (a) Zhang, W.-L.; Lin, C.-S.; Geng, L.; Li, Y.-Y.; Zhang, H.; He, Z. Z.; Chen, W.-D. *J. Solid State Chem.* **2010**, *183*, 1108−1113. (b) Adam, L.; Guesdon, A.; Raveau, B. *J. Solid State Chem.* **2008**, *181*, 3110−3115. (c) Ranmohotti, K. G. S.; Mo, X.; Smith, M. K.; Hwu, S.-J. *Inorg. Chem.* **2006**, *45*, 3665−3670. (d) Mo, X.; Etheredge, K. M. S.; Hwu, S.-J.; Huang, Q. *Inorg. Chem.* **2006**, *45*, 3478−3480. (e) Belik, A. A.; Azuma, M.; Matsuo, A.; Whangbo, M.-H.; Koo, H.-J.; Kikuchi, J.; Kaji, T.; Okubo, S.; Ohta, H.; Kindo, K.; Takano, M. *Inorg. Chem.* **2005**, *44*, 6632−6640.